Morphology Control in Films of Isoindigo Polymers by Side-Chain and Molecular Weight Effects

Morphology Control in Films of Isoindigo Polymers by Side-Chain and Molecular Weight Effects

Caroline Grand,[1†] Wojciech Zajaczkowski,[2] Nabankur Deb,[3§] Chi Kin Lo,[1] Jeff L. Hernandez,[1] David G. Bucknall,[3‡] Klaus Müllen,[2] Wojciech Pisula,[2,4] John R. Reynolds[,1]*

1. School of Chemistry and Biochemistry, School of Materials Science and Engineering, Center for Organic Photonics and Electronics, Georgia Tech Polymer Network, Georgia Institute of Technology, Atlanta, Georgia 30332-0400, United States.

2. Max Planck Institute for Polymer Research, Ackermannweg 10, 55128 Mainz, Germany.

3. School of Materials Science and Engineering, Center for Organic Photonics and Electronics, Georgia Tech Polymer Network, Georgia Institute of Technology, Atlanta, Georgia 30332-0400, United States.

4. Department of Molecular Physics, Faculty of Chemistry, Lodz University of Technology, Zeromskiego 116, 90-924 Lodz, Poland.

KEYWORDS. Isoindigo, Donor-Acceptor Polymers, Thin Film Morphology, Organic Field-Effect Transistors, Polymer Fullerene Blends, Bulk Heterojunction Solar Cells, Organic Photovoltaics

ABSTRACT. The performance of devices relying on organic electronic materials, such as organic field-effect transistors (OFET) and organic photovoltaics (OPV), is strongly correlated to the morphology of the conjugated material in thin films. For instance, several factors such as polymer solubility, weak intermolecular forces between polymers and fullerene derivatives as charge acceptors, and film drying time impacts phase separation in the active layer of a bulk heterojunction OPV device. In an effort to probe the influence of polymer assembly on morphology of polymer thin films and phase separation with fullerene derivatives, five terthiophene-*alt*-isoindigo copolymers were synthesized with alkyl side-chains of varying lengths and branching on the terthiophene unit. These P[T3(R)-iI] polymers were designed to have similar optoelectronic properties, but different solubilities in *o*-dichlorobenzene (oDCB), and were predicted to have different tendencies for crystallization. All polymers with linear alkyl chains exhibit similar thin film morphologies as investigated by grazing-incidence wide-angle X-ray scattering (GIWAXS) and atomic force microscopy (AFM). The main differences in electronic and morphological properties arise when P[T3(R)-iI] is substituted with branched 2-ethylhexyl (2EH) side-chains. The bulky 2EH substituents lead to a blue-shifted absorption, a lower ionization potential and reduced ordering in polymer thin films. The five P[T3-iI] derivatives span hole mobilities from 1.5×10^{-3} cm^2 V^{-1} s^{-1} to 2.8×10^{-2} cm^2 V^{-1} s^{-1} in OFET devices. In OPV devices, the 2EH-substituted polymers yield open-circuit voltages of 0.88 V in BHJ devices, yet low short-circuit currents of 0.8 mA cm^{-2}, which is explained by the large phase separation observed by AFM in blends of P[T3(2EH)-iI] with $PC_{71}BM$. In these P[T3(R)-iI] systems, the propensity for the polymers to self-assemble prior to aggregation of $PC_{71}BM$ molecules was key to achieving fine phase separation and increased short-circuit currents, eventually resulting in power conversion efficiencies of 5% in devices processed using a single solvent.

INTRODUCTION

Organic electronic devices in general, and organic field-effect transistor (OFET) or organic photovoltaic (OPV) devices in particular, have emerged as a complementary technology for sensors and energy generation from light-weight and flexible modules, in addition to rapid energy payback time of less than six months for OPVs compared to over a year for silicon-based solar cells.[1] However, significant progress needs to be achieved in order to bring organic electronic technology to commercial viability.[2] From a technical standpoint, most of the research has been focused on developing new π-conjugated polymers,[3-6] where two main factors can be modified on the polymer chain to influence structure-property relationships. The first is varying the nature and composition of donor or acceptor moieties along the backbone to tune optoelectronic properties. The second is changing the structure of solubilizing side-chains,[7-9] where longer and branched alkyl chains improve solubility and processability, but are also expected to disrupt interchain π-interactions, and as such limit device performance.[10, 11] For example, both of these factors come into effect in bulk heterojunction (BHJ) blends with fullerene derivatives as the electron accepting materials for OPV devices. Polymeric donor materials are designed by focusing on donor-acceptor interactions along the backbone to tune light absorption[12] and exciton dissociation at the interface with a fullerene acceptor,[13] where solubilizing side-chains also have a large impact on charge transfer[14] and morphology.[15, 16] In OPV devices based on fullerene derivatives, phase separation between the polymer-rich domains and the fullerene-rich aggregates, with dimensions on the order of 10 to 30 nm due to the typical exciton diffusion length, is one of the many requirements for efficient charge generation from absorbed photons.[17-19] In particular, the correlation between polymer structure and the resulting phase separation in the BHJ blend is not yet clear; however some trends can be distinguished by considering the impact of backbone and side-chain flexibility

on phase separation.[20] Figure 1 reviews previous work and highlights the impact of polymer structure and processing solvent on phase separation in blends with [6,6]-phenyl C_{71}-butyric acid methyl ester ($PC_{71}BM$), with systems leading to phase separated domains with sizes (as determined by atomic force microscopy) above 50 nm in red, and systems leading to phase separated domains with sizes below 50 nm in green. The x-axis attempts to quantify backbone flexibility by taking the ratio of double bonds involved in the π-conjugation length to the number of σ-bonds between heterocycles. The y-axis takes into account the impact of branching along the alkyl side-chains on polymer solubility.

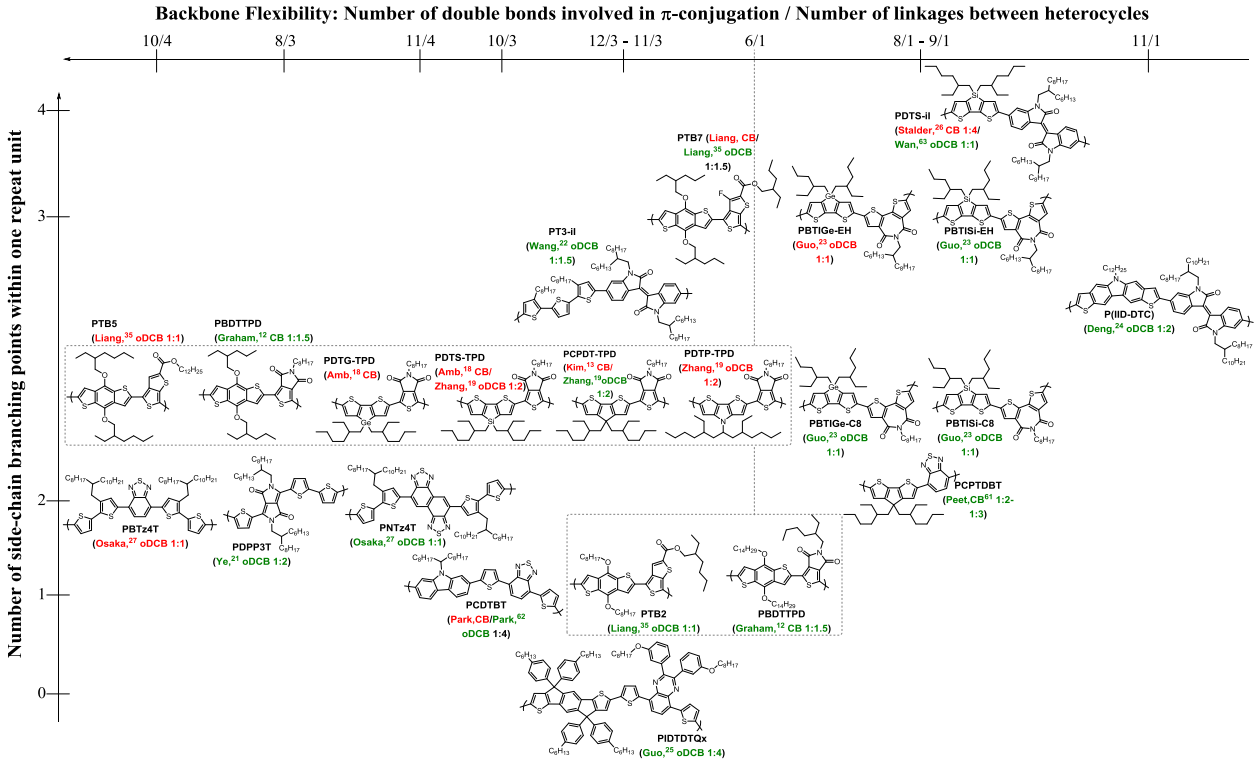

Figure 1. Selection of previously reported polymer structures for polymer:fullerene blends in OPV devices (polymer:fullerene ratio is reported in the brackets), where solvents leading to small phase separation with fullerenes are written in green (domains < 50 nm) and solvents leading to large phase separation are in red (domains ≥ 50 nm).

Figure 1 highlights that spin-coating blends with fullerene derivatives from *o*-dichlorobenzene (oDCB) seems to yield smaller features than blends cast from chlorobenzene (CB) for the same polymer structure, as seen for PCDTBT, PTB7 or PCPDT-TPD, as well as, with some exceptions, in blends based on PDTS-TPD.[21, 22] It is important to note that the two PDTS-TPD systems processed from CB and oDCB were reported by two different groups in separate publications, highlighting that other processing parameters will also impact the resulting thin film morphology. The decrease in feature size when changing the solvent from CB to oDCB was also highlighted in earlier publications focusing on MDMO-PPV:$PC_{71}BM$ blends.[23] Furthermore, polymers containing diketopyrrolopyrrole (DPP),[24] terthiophene[25] or rigid units such as dithienocarbazole in the backbone of IID-DTC,[26, 27] tend to result in finer phase separation even when sterically hindered groups are appended to the structure, as is the case for PIDTDTQx.[28] On the other hand, structures with branched side chains on fused bithiophene rings cause large phase separation in blends cast from CB,[21, 29] and also from oDCB as is the case with PBTiGe-EH and PDTP-TPD materials.[22, 26] The work of Guo *et al*.[26] also demonstrates that there is a decrease in polymer crystalline ordering in thin films going from PBTiSi to PBTiGe backbones. Similarly, work by Osaka *et al*.[30] demonstrates that a change from benzothiadiazole in PBTz4T to naphthobisthiadiazole in PNTz4T results in a decrease in phase separation in BHJ blends when cast from oDCB coupled with an increase in polymer ordering in thin films.

Thermodynamically, phase separation can be described by a ternary phase diagram, and three phase transition processes can be schematically derived: liquid-liquid, solid-liquid and/or solid-solid transitions as investigated by Kouijzer *et al*.[31] Kinetically, Pearson *et al*.[32] investigated the drying process in PCDTBT blends in oDCB, and found that the phase separation is controlled by

fullerene precipitation followed by polymer ordering for blends with a high content of fullerene (80%). Based on this previous work, it is hypothesized that films cast from CB tend to follow liquid-liquid demixing causing large phase separation, while oDCB allows for longer drying times of the films, enabling polymer or fullerene aggregation (or solid-liquid demixing) as the layer is drying, which can yield smaller domains in the dried BHJ.[33-35] In the case of a BHJ with a high polymer content (> 30%) cast from oDCB, the morphology is hypothesized to be controlled by the ability of the polymer chains to form aggregated fibrils through π-interactions (where the width of the fibrils can be further dictated by the polymer solubility[36, 37]); when these interactions are hindered, fullerene aggregate growth would lead to large fullerene domains embedded in a polymer matrix, as seen for blends with high fullerene content.[33] This hypothesis only takes into account interchain polymer interactions, and not fullerene:polymer interactions, which needs to be considered especially in the case of fluorinated polymers, as shown by the different phase separation in blends of PTB5 compared to PTB7 (Figure 1).[38]

In order to investigate the correlation between polymer packing, morphology and device performance, we synthesized a family of five copolymers of terthiophene-*alt*-isoindigo with varying side-chains on the terthiophene unit, P[T3(R)-iI] as seen in Scheme 1, in order to increase polymer solubility, whilst minimizing any impact on optoelectronic properties. These polymers were designed to exhibit increased solubility in oDCB with increasing length of the side-chain, while minimizing changes in the packing structure of the polymers in thin-films, to probe the effect of polymer solubility on phase separation with fullerenes. The polymer substituted with 2-ethylhexyl side-chains was included in this study to understand how polymer ordering also impacts charge carrier mobilities in OFETs and phase separation in OPV active layers. The terthiophene-isoindigo backbone was targeted for this study based on the work of Wang *et al.*[25, 39] and Ho *et*

al.[40] who have demonstrated that poly(terthiophene-*alt*-isoindigo) P[T3-iI] exhibits an energy gap of 1.5 eV for light absorption at near-infrared wavelengths, while maintaining a suitable energy in the excited state for exciton dissociation in PCBM based BHJs, leading to efficiencies above 6% in conventional OPV devices. Stalder et *al.* have studied the same polymer backbone in OFET devices demonstrating a hole mobility of 0.05 $cm^2 V^{-1} s^{-1}$.[41] This family of P[T3(R)-iI] polymers was used to investigate both relationships between polymer packing and transport in OFETs and also phase separation in blends with fullerene derivatives in OPVs. The results show result, P[T3(2EH)-iI] is processable in common organic solvents such as tetrahydrofuran, chloroform, CB and oDCB. By comparison, P[T3(C6)-iI] demonstrates high solubility (> 8 mg/mL) in chloroform, but limited solubility in oDCB at room temperature. The change in polymer structure and its impact on morphology and charge transport in OFET and phase separation in OPV devices, are explored by either modifying the alkyl side-chains or varying molecular weight of the P[T3(C12)-iI] polymer, without modifying the conjugated polymer backbone.

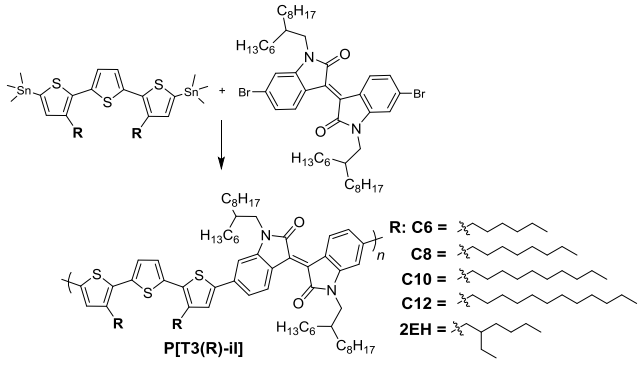

Scheme 1. Synthesis of P[T3(R)-iI] derivatives with alkyl side-chains of varying length and branching on the terthiophene unit.

In this contribution, we demonstrate that linear side chains on the terthiophene (T3) unit improve nanostructured order compared to functionalizing T3 with branched 2-ethylhexyl (2EH) chains. Coupled with favorable orientation of the polymer backbones, as observed by grazing incidence wide-angle X-ray scattering (GIWAXS), ordering in these *n*-alkyl substituted derivatives is expected to improve charge carrier transport in OFET devices, while polymer processability is increased. This is also true for blends with $PC_{71}BM$ in OPV devices, where P[T3(C8)-iI] exhibits higher performance with increased processability compared to P[T3(C6)-iI]. On the other hand, 2EH side chains result in an increased ionization potential of the polymer due to torsion along the backbone, which is reflected in a high open-circuit voltage (0.8V) in the corresponding OPV devices, and large phase separated domains between the P[T3(2EH)-iI] polymer and the $PC_{71}BM$. Moreover, the influence of polymer molecular weight on its packing and charge transport in OFETs is discussed, with higher molecular weight polymers yielding enhanced hole mobilities in OFET devices. These small structural changes in the polymer substitution underline some of the mechanisms which can be used to explain morphology in polymer films and blends with fullerene derivatives.

RESULTS AND DISCUSSION

Synthesis and Optoelectronic Properties. To demonstrate the influence of side-chain structure on solubility and morphology, P[T3(R)-iI] derivatives were synthesized using Stille polycondensation with *n*-hexyl (C6), *n*-octyl (C8), *n*-decyl (C10), *n*-dodecyl (C12) and 2-ethylhexyl (2EH) side-chains on the terthiophene unit, while maintaining a 2-hexyldecyl side-chain on the isoindigo unit to ensure solubility during polymerization. Details of the synthesis can be found in the Supporting Information (SI). All polymerization mixtures were fractionated through Soxhlet extraction. In the case of P[T3(C12)-iI] Soxhlet extraction yielded two fractions

with different solubilities: a lower molecular weight fraction (C12, M_n = 41 kDa) soluble in dichloromethane and a higher molecular weight fraction soluble in chloroform (C12, M_n = 65 kDa), both of which are studied here. Polymer purity, assessed by elemental analysis, is reported in Table S1 (SI) and polymer molecular weights, as estimated by gel permeation chromatography (GPC), are summarized in Table 1. The GPC chromatograms can be found in Figure S11 of the Supporting Information.

Table 1. Purity Based on Organic Composition, Molecular Weight, Solubility, Electrochemical, and Optical Properties of the P[T3(R)-iI] polymers.

R	ΔEA[a]	Mn/Mw, PDI[b] (kDa), TCB	Solubility[c] (mg/mL)	E_{gap}^{abs} [d] (eV)	E_{gap}^{DPV} [e] (eV)	E_{ox}^{onset} (V)/ IP[f] (eV)	E_{red}^{onset} (V)/ EA[g] (eV)
C6	0.3%	80/207, 2.6	2 ± 1	1.57	1.65	0.48/-5.58	-1.17/-3.93
C8	0.2%	70/146, 2.1	10 ± 2	1.57	1.68	0.48/-5.58	-1.20/-3.90
C10	0.2%	61/126, 2.1	12 ± 2	1.55	1.54	0.50/-5.60	-1.04/-4.06
C12							
65k	0.8%	65/125, 1.9	12 ± 2	1.58	1.71	0.45/-5.55	-1.26/-3.84
41k	0.5%	41/103, 2.5	21 ± 5	1.58	1.66	0.45/-5.55	-1.21/-3.89
2EH	0.4%	53/126, 2.4	27 ± 5	1.60	1.88	0.71/-5.81	-1.17/-3.93

[a]maximum difference between theoretical and measured elemental composition for C, H, N and S atoms (full elemental analysis results can be found in SI), [b]molecular weight distribution estimated by GPC in 1,2,4-trichlorobenzene (TCB) at 135 °C against polystyrene standards, [c]solubility in oDCB measured at room temperature, [d]optical energy gap calculated from absorption onset of polymer films, [e]energy gap calculated from oxidation and reduction onsets in DPV trace, [f]ionization potential and [g]electron affinity measured by DPV vs. Fc/Fc^+.

The solubility of the polymers in oDCB was measured at room temperature by removing insoluble material from a saturated solution at room temperature via a centrifuge, and comparing the absorption of the supernatant to a calibration UV-vis curve in order to determine the amount of solubilized polymer (Figure S1). Table 1 shows that solubility can be tuned by varying the

length and branching of the side-chain, as well as by changing the molecular weight of the polymer. The synthesized P[T3(R)-iI] derivatives are able to span polymer solubilities ranging from 2 mg/mL to 27 mg/mL in oDCB at room temperature.

Thermal analysis and UV-visible-NIR absorption spectroscopy were used to study the impact of alkyl chain substitution on polymer stability, semicrystallinity, and optical properties. All polymers demonstrate thermal stability up to 350 °C as determined by thermogravimetric analysis (TGA) (Figure S2a). Further thermal analysis of P[T3(C6)-iI] and P[T3(2EH)-iI] by differential scanning calorimetry (DSC) shows a melting transition at 287 °C in the case of P[T3(C6)-iI] with no crystallization peak upon cooling, and a melting transition at 180 °C with a crystallization peak at 150 °C for P[T3(2EH)-iI] (Figure S2b-c). Other reports indicate a peak melting temperature for P[T3(C8)-iI] at 289 °C,[39] which points to the fact that the melting point transition temperature is decreased by the disorder afforded by the branched 2EH side-chains. This change in polymer ordering with changes in side-chains is also supported by GIWAXS results (*vide infra*).

Furthermore, it is expected that variations in the length of the linear side-chains will have minimal impact on the absorption properties of P[T3-iI], but that steric hindrance caused by 2EH chains will lead to an increase in backbone torsion and reduction in conjugation length. This effect was previously reported in the case of polythiophenes where torsion along the backbone caused by steric hindrance from alkyl chains led to an increased energy gap and increased ionization potential (IP).[42] Here, UV-vis-NIR spectroscopy shown in Figure 2a, reveals strong similarity in the oDCB solution absorption of P[T3-iI] with linear side-chains, and a blue shifted absorption maximum for P[T3(2EH)-iI]. Considering the absorption of solid films of the polymers as shown in Figure 2b, the blue shift remains in the onset of absorption for P[T3(2EH)-iI] compared to the other polymers, indicating an increase in the energy gap as was previously reported in thiophene-

based polymers. Furthermore, a distinct aggregation shoulder is visible in the solid state for all five polymers with linear alkyl chains, which highlights a possibly different solid-state packing between polymers where T3 is substituted with a linear alkyl chain compared to P[T3(2EH)-iI] with all-branched side-chains.

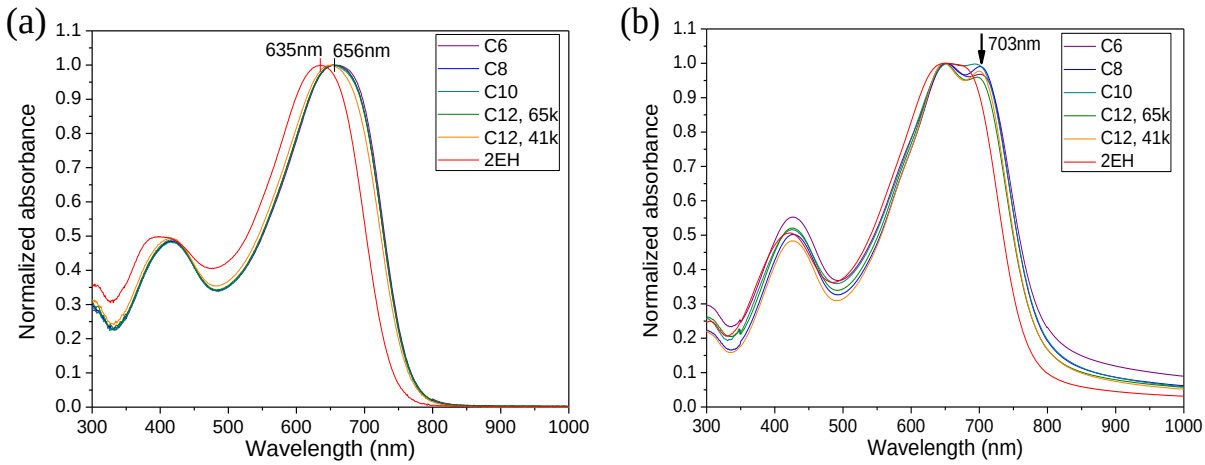

Figure 2. Normalized UV-vis absorption spectra of P[T3(R)-iI] polymers: (a) in oDCB solution; (b) as spun-cast thin films on glass.

The observed increase in energy gap of P[T3(2EH)-iI] in the solid state was further investigated by carrying out differential pulse voltammetry (DPV) on polymer thin films deposited on Pt electrodes in an electrolyte composed of 0.1M $TBAPF_6$ in acetonitrile. Onsets of oxidation and reduction were determined relative to Fc/Fc^+, and the IP and electron affinity (EA) were estimated using 5.1 eV below vacuum as the potential of Fc/Fc^+.[43] Little change is observed for polymers with linear chains with IP around 5.6 eV; however, the IP of P[T3(2EH)-iI] is increased by 0.2 eV to 5.8 eV (Figure S3). This increase in IP with branched side-chains is expected to increase the open-circuit voltage in OPV devices,[42] as discussed in a following paragraph.

Polymer Packing Determination by Grazing Incidence Wide-Angle X-Ray Scattering (GIWAXS). Besides having an impact on the optoelectronic properties, the 2EH side chains are expected to impact polymer packing as seen in the lower DSC melting point and in the blue-shifted solid-state UV-visible-NIR spectrum. To further investigate this effect seen in thin films, grazing incidence wide-angle X-ray scattering (GIWAXS) was performed on spun-cast thin films of the polymers from oDCB solutions on silicon wafers before and after annealing at 200 °C (Figures 3 and 4). After integration over a quadrant of the detector, line shape analysis can be conducted using Gaussian functions to fit the scattering peaks, where the peak positions are attributed to the (hkl) scattering planes and the full widths at half maximum (FWHM) give indications on the crystallinity of the scattering peak and on the crystallite size.

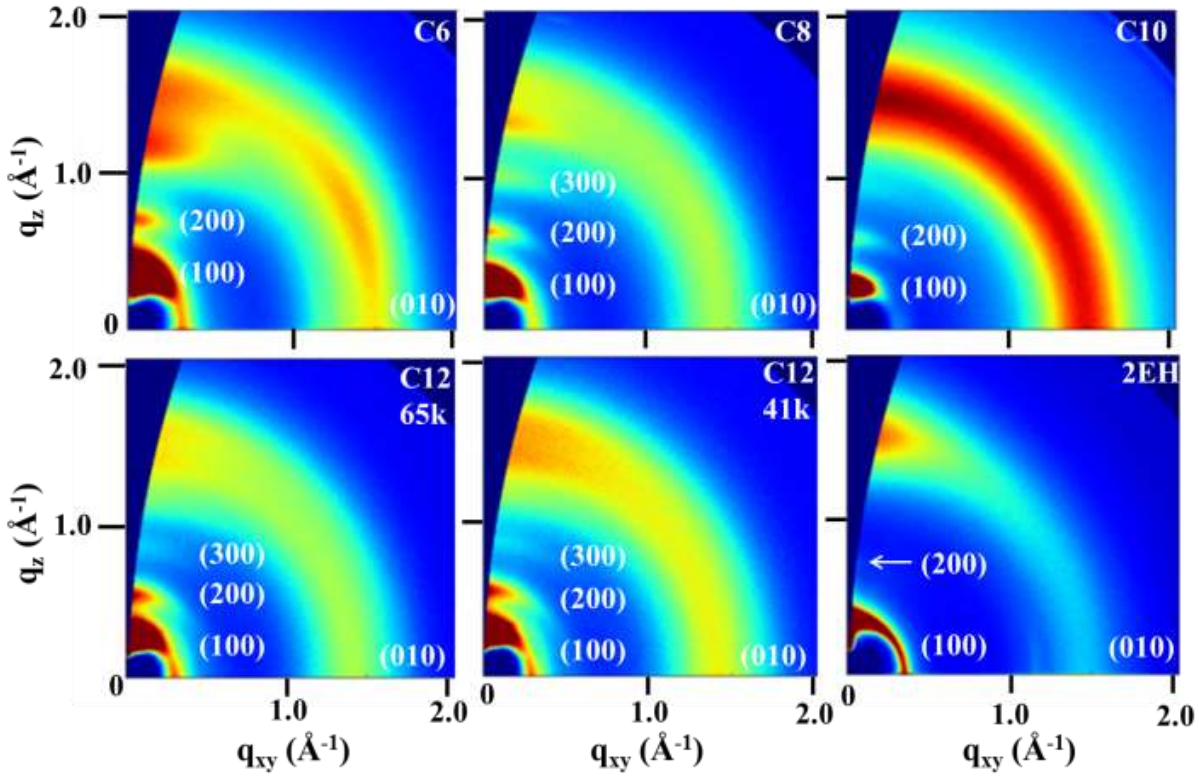

Figure 3. GIWAXS patterns of as-cast films of P[T3(R)-iI] from oDCB.

A first observation from Figure 3 is the mixed organization of the polymer chains relative to the substrate. P[T3(R)-iI] with C8 and C12 chains reveal features in the GIWAXS pattern characteristic for lamellar stacking both out-of-plane and in-plane. The out-of-plane lamellar orientation is indicated by (h00) reflections along the q_z axis, while a broad wide-angle scattering intensity also located along the q_{xy} axis of the pattern, possibly from (010) planes, suggests some in-plane orientation of the lamellar population. Coexistence of both lamellar orientations is not untypical and has been reported for several high performance polymers.[44, 45] As cast film of P[T3(C6)-iI] indicate the presence of a 3rd population with the unit cell planes tilted towards the surface with an angle around 30° at q values of 1.55 $Å^{-1}$, corresponding to a characteristic distance of 4.1 Å. It is possible that this scattering peak may be due to π-stacking, as 2D-WAXS indicates a π-stacking distance of 3.9 Å (Table S2). Moreover, although P[T3(C10)-iI] assembles with the polymer backbone edge-on to the substrate with several orders of (h00) peaks visible in the out-of-plane direction, the scattering halo in the π-stacking region, with a slight increase in intensity along the q_z axis, is indicative of low intralayer ordering and of a slight preferential orientation of the (010) peak along q_z. P[T3(2EH)-iI] exhibits a similar scattering pattern to the P[T3(R)-iI] polymers with linear chains, although the higher order (h00) reflections are not as intense along the q_z axis. By comparison to polymers with linear alkyl chains, P[T3(2EH)-iI] films also scatter along the q_z axis, but at an increased characteristic distance. This is indicative of intralayer ordering where the stacking distance is larger than that of the polymers with linear alkyl chains, due to the more twisted backbones induced by the bulkier 2EH side-chain. These bulkier branched chains yield less ordered structures, which in turn can explain the lack of an aggregation peak at 700 nm in the solid-state UV-visible spectrum of P[T3(2EH)-iI] in Figure 2.

Since the morphology of the polymers in the as-cast thin films will tend to be kinetically trapped, annealing studies were conducted at 200 °C (maximum temperature accessible by the GIWAXS setup) to understand the evolution of polymer ordering towards a more thermodynamically favored morphology, although there may remain kinetically trapped polymorphs that cannot be changed or healed by annealing. Figure 4 illustrates the GIWAXS results from the polymer thin films after thermal annealing at 200 °C under a helium atmosphere for 10 min. An example is given in Figure S4 of the changes in scattering of thin films based on P[T3(C6)-iI] at various temperatures in a thermal annealing cycle. As the temperature is increased, the peak intensities and the overall scattering peak area decreases, indicating a loss of ordering in the film and the possibility for the chains to ultimately reorganize to a more thermodynamically favored packing structure. For all polymers, an increase in the more thermodynamically favored edge-on population of the π-stacks is observed,[46] and quantified by the Herman orientation factor (HOF) for the (100) peak as reported in Table 2. The HOF quantifies the extent of orientation of the lamella relative to the substrate, with out-of-plane lamella (lamellar (h00) peaks along q_z) described by a HOF of 1, and in-plane lamella (lamellar (h00) peaks along q_{xy}) leading to HOF of -0.5, while randomly oriented crystals have a HOF of zero (details can be found in the SI). As seen in Table 2, a HOF of 0.5 as is the case here points to a majority of the population having lamellar packing out-of-plane (i.e. π-stacking edge-on) with some chains having lamellar packing in-plane (i.e. π-stacking face-on). Orientation has been shown to have a substantial impact on transport properties in OFET devices for some polymer systems,[47-49] and it is expected that this increase of π-interactions parallel to the substrate after thermal annealing will lead to increased charge carrier mobility in OFET devices. However this hypothesis is not always true depending on the polymer system as pointed out in a review by Sirringhaus.[50] It is also important to note that in blends with

fullerenes, polymer orientation relative to the substrate may have some impact of OPV device parameters;[51] however the effect of polymer orientation at electrode interfaces is difficult to deconvolute from phase separation between the polymer and fullerene and polymer orientation at the polymer:fullerene interface.[14]

Table 2. Characteristics of polymer P[T3(R)-iI] packing in as-cast and thermally annealed thin films as a function of alkyl chain substitution.

	GIWAXS As-cast			GIWAXS Annealed				
Sample	π^a (Å)	Lamellar[b] (Å)	$L_{c,d}$[c] (Å)	π^a (Å)	$L_{c,\pi}$[d] (Å)	Lamellar[b] (Å)	$L_{c,d}$[c] (Å)	HOF
C6	4.1	18	105	3.7	57	19	129	0.5
C8	4.2	19	122	3.7	61	20	158	0.5
C10	4.2	20	125	3.8	42	21	167	0.5
C12, 65k	4.3	21	113	3.7	55	22	205	0.5
C12, 41k	4.3	21	116	/	/	22	207	0.5
2EH	4.3	17	152	4.2	/	18	202	0.6

[a]π: π-π distances, [b]Lamellar: Chain-to-chain distances, [c]$L_{c,d}$: Coherence length along chain-to-chain direction, [d]$L_{c,\pi}$: Coherence length within π-stacks.

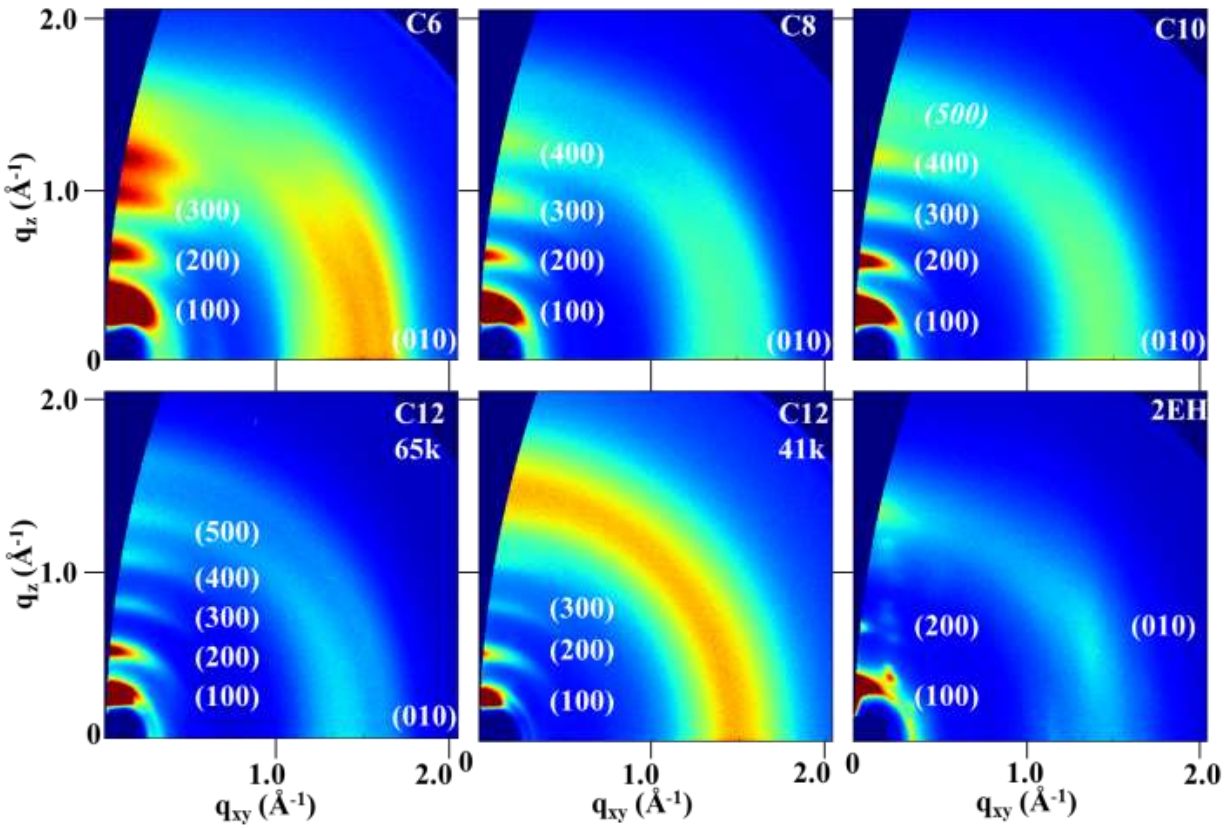

Figure 4. GIWAXS of P[T3(R)-iI] polymer films annealed at 200 °C for 5 min and cooled to room temperature.

In contrast to the as-cast films, ordering in the thin films is increased with thermal annealing as shown by the increased number of higher (h00) order peaks along q_z and the increase in coherence length (L_c) as discussed in a subsequent paragraph. In particular, 2EH exhibits crystalline peaks along the q_{xy} = 0.25 Å^{-1} direction that the other polymers do not display. In the case of 2EH, the thin film was heated past the polymer's melting temperature of 180°C, and slow cooling around its crystallization temperature allowed for additional crystalline domains to form. Off-equatorial peaks are also possibly arising from side chain crystallization as noted in the case of PBTTT and P(NDI2OD-T2) polymer chain crystals in isotropic thin films.[52-54] Moreover, in the

polymers with linear chains, the π-stacking distances decrease by 0.1-0.5 Å and the lamellar distances increase by 1-2 Å. This can be understood by thermally induced planarity of the backbones, leading to the polymer backbone getting closer and interacting more strongly with one another and the side chains now extending perpendicular to the backbone, rather than at an angle. The presence of a new peak along the q_{xy} axis, noticeable in particular in films of C6, along with the presence of two melting peaks in the DSC (Figure S2) seems to indicate the presence of two polymorphs for these polymers. Scherrer analysis was conducted to quantify the coherence length L_c (or crystal size) in the annealed films (details can be found in the SI). In the π-stacking direction, Lc,π is calculated to be 4-6 nm, which indicates that order can be found over 10 to 16 polymer backbones for the least soluble polymers.

To further verify our assumptions for peak assignment in the GIWAXS data, 2D-WAXS was obtained on extruded polymer fibers annealed at 120 °C and 200 °C (Figure S5). 2D-WAXS analysis investigates bulk structural organization and highlights the fact that P[T3(R)-iI] polymers assemble in chain-to-chain, lamellar structures oriented in the extrusion direction as shown by scattering in the equatorial direction with both chain-to-chain lamellae and π-stacks oriented perpendicular to the extrusion direction. Similarly to the GIWAXS data, 2EH goes through a melting transition below 200 °C, and as such exhibits diffuse anisotropic rings after annealing at 200 °C compared to the other polymers. The characteristic distances were determined from line integration along the equatorial direction, and the data is summarized in Table S2. In general, after annealing at 200 °C, the packing distances in the bulk are slightly lower than what is observed in thin films annealed at the same temperature and could be due to the strain of the extrusion process or to the lack of influence of a substrate on polymer packing.

From the 1D-integrated plots shown in Figure S6, variations in 2D-WAXS scattering along the equatorial direction for the six P[T3(R)-iI] polymers are observed with increased annealing temperature. Although no change is observed in the 2D-WAXS pattern of P[T3(2EH)-iI] after annealing at 120 °C, annealed fibers of the other five P[T3(R)-iI] polymers exhibit higher order (h00) scattering peaks in their 2D-WAXS pattern compared to as extruded fibers, as was also observed in the GIWAXS data in the case of P[T3(R)-iI] thin films. In the case of fibers of P[T3(R)-iI] with linear chains, the peak associated with π-stacking becomes narrower after thermal annealing at 200 °C, indicating an increase in the size of the crystal domains. Moreover, in annealed samples of P[T3(C8)-iI], P[T3(C10)-iI] and P[T3(C12)-iI] (65k and 41k), both the GIWAXS and 2D-WAXS data show a splitting of the (100) peak at low q after thermal annealing (Figure S6) as pointed out in a previous paragraph. It is difficult to rationalize the presence of the two peaks, as no further peak splitting is observed for higher order (h00) peaks. It is possible that the two higher order peaks are buried under the broader (h00) peaks. Similar splitting of the (100) diffraction peaks was observed by Rogers *et al.*[55] in PCDTBT films and was attributed to two different crystal structures, which is again reminiscent of the two peaks in the DSC trace of C6. Comparing the 2D-WAXS of the fibers after annealing at 120 °C, the π-stacking distance remains at 3.9 Å regardless of the alkyl side-chain length, but is increased to 4.2 Å when 2EH is used. The impact of the length of the alkyl side-chain can be observed in the chain-to-chain distance, where both C6 and 2EH side chains yield lamellar distances of 19 Å, and the lamellar distance increases with chain length up to 24 Å in the case of the two P[T3(C12)-iI] polymers.

Combining the structural information obtained on as-processed films and fibers, it is concluded that polymers with linear chains on the terthiophene unit exhibit increased short-range ordering in thin films compared to P[T3(2EH)-iI] as observed by UV-vis spectroscopy. Variations in polymer

packing are made more visible with annealing, where higher order peaks appear in samples of the polymers with linear side chains while P[T3(2EH)-iI] only shows a crystallization transition after annealing at 200 °C with no increased ordering at temperatures below its melting transition. This points to the propensity of the P[T3(R)-iI] polymer chains to crystallize when they are functionalized with linear alkyl side chains; however, this effect is hindered in the presence of the bulkier 2EH side chains.

Transistor Fabrication and Characterization. In order to probe the effect of polymer packing on charge transport, bottom-gate/bottom-contact OFET devices were fabricated on heavily doped silicon wafers covered with HMDS-modified SiO_2. Gold electrodes were patterned to form 10 μm long and 700 μm wide channels. The polymer layers were drop-cast from a 4.4 mg/mL solution in oDCB at 120 °C onto the substrates maintained at 120 °C, and subsequently annealed at 120 °C for 1h. Table 3 summarizes the OFET performance obtained across the polymer series (Figure S7 shows the transfer and output curves for P[T3(C6)-iI]-based OFETs). It is important to note the difference in processing between the films used to obtain GIWAXS data (polymer films spun-cast on silicon wafers and annealed at 200 °C) and the active films in OFET devices (polymers drop-cast on HMDS-modified silicon wafers and annealed at 120 °C); however 2D-WAXS data was obtained using similar annealing conditions and is used to draw trends linking polymer structure, morphology and device performance.

A first observation is that all polymers exhibit ambipolar transport, except for C8, with electron mobility being one to two orders of magnitude lower than hole mobility, except in the case of 2EH where the hole and electron mobility are 4.0×10^{-3} and 1.4×10^{-3} $cm^2\ V^{-1}\ s^{-1}$, respectively. This ambipolar transport was observed in several isoindigo-containing systems[56] and is thought to arise from interchain overlap of isoindigo units shown by solid-state NMR in the work of Stalder *et al.*

on isoindigo polymers.[41] For C6, C10 and C12 (65 kDa) polymers, hole mobility is measured to be between 2.3×10^{-2} and 2.8×10^{-2} $cm^2 V^{-1} s^{-1}$, showing little influence of the length of the side-chain and of the chain-to-chain distance on hole mobility. However, comparison of the two fractions of P[T3(C12)-iI] highlights an increase of the hole mobility by an order of magnitude when the higher molecular weight fraction is used in devices, with hole mobilities of 2.0×10^{-3} $cm^2 V^{-1} s^{-1}$ for the lower molecular weight polymer. This increase in hole mobility with increasing molecular weight has been observed previously,[57, 58] and this work further supports the influence of molecular weight on carrier mobilities in OFET devices. The hole mobility also drops to 4.0×10^{-3} $cm^2 V^{-1} s^{-1}$ in devices fabricated with 2EH. Interestingly, the low mobility observed in lower molecular weight polymer and in polymers with all-branched side chains correlates with the reduction in coherence lengths, although charge transport cannot only be linked to crystalline domains, but is limited by arrangements of the polymer chains in amorphous regions of the thin film.[58, 59] The results from OFET devices based on P[T3(C8)-iI] do point out an example of a limitation between 2D-WAXS and GIWAXS results and OFET charge mobilities, as was also shown previously for a family of isoindigo-based polymers.[41] Indeed, GIWAXS results for P[T3(C8)-iI] are on par with results for P[T3(C6)-iI] or P[T3(C10)-iI]; however the hole mobility is an order of magnitude lower and no electron mobility is measured in devices based on P[T3(C8)-iI]. It is possible that in the case of P[T3(C8)-iI] the non-crystalline regions, which are not characterized by our current X-ray scattering analysis, have a greater impact on carrier mobility than in P[T3(C6)-iI] or P[T3(C10)-iI] devices.[60, 61] Furthermore, interfacial phenomena have a great impact on the mobilities measured in OFET devices, while 2D-WAXS probes polymer packing in the bulk[57] and GIWAXS is investigating polymer packing over the full film thickness under the conditions used here.[54, 62]

Table 3. Hole (μ_h) and electron (μ_e) mobilities in OFET devices and corresponding OFET threshold voltages V_{th} after annealing at 120 °C.

P[T3(R)-iI]	μ_h ($cm^2V^{-1}s^{-1}$)*10^{-3}	V_{th}^h (V)	μ_e ($cm^2V^{-1}s^{-1}$)*10^{-3}	V_{th}^e (V)
C6	25.8 ± 3.1	-20 ± 3	3.9 ± 0.3	49 ± 12
C8	6.8 ± 1.4	-26 ± 5	-	-
C10	23.3 ± 1.8	-20 ± 4	2.9 ± 0.6	43 ± 8
C12, 65k	28.4 ± 3.3	-23 ± 2	0.1 ± 0.0	34 ± 12
C12, 41k	1.5 ± 0.2	-25 ± 4	0.9 ± 0.2	44 ± 6
2EH	4.3 ± 0.6	-19 ± 1	1.4 ± 0.3	60 ± 1

Statistical data was obtained over 10 measurements, except in the case of n-type OFET devices based on P[T3(C6)-iI], where 5 measurements were conducted to obtain electron transport characteristics.

Solar Cell Device Fabrication and Testing. The photovoltaic properties of the six polymers were examined in BHJ devices with (6,6)-phenyl-C_{71}-butyric acid methyl ester ($PC_{71}BM$) as the electron acceptor. All solar cell devices were fabricated and tested under inert atmosphere and the photocurrent was measured under simulated AM 1.5G solar illumination at an irradiation intensity of 100 mW cm^{-2}. Blends of polymer:$PC_{71}BM$ at a 1:1.5 ratio were deposited via spin-coating from oDCB solutions (without any solvent additives such as DIO) at 80 °C onto ITO glass coated with a PEDOT:PSS layer, and layers of calcium and aluminum were sequentially deposited on top of the active layer to form the cathode. The devices were not fully optimized, but rather fabricated in the same fashion, relying on optimized parameters for P[T3(C6)-iI][63] without the use of processing additives to understand the impact of the polymer properties alone, and tuning film thickness to achieve comparable light absorption in devices based on the other five polymers (see Figure S8) for direct comparison of the effect of the side-chain and molecular weight in the BHJ devices. Although light absorption is targeted to be similar across all devices, an increase in film thickness

will also increase the probability of recombination within the active layer due to changes in the morphology of the bulk,[64] space-charge effects and short carrier lifetimes.[65]

Devices fabricated using P[T3(C6)-iI] and P[T3(C8)-iI] achieved average power conversion efficiencies (PCE) of 5.1% and 5.2% respectively (Table 4), in agreement with previously reported OPV devices prepared without additives.[25] Compared to other P[T3(R)-iI] polymers, the increased short-circuit current (J_{sc}) and fill factor (FF) leads to these higher efficiencies in P[T3(C6)-iI] and P[T3(C8)-iI] blends. In particular, the FF increases with decreasing active layer thickness, due to decreased probability for charge recombination in thinner films as discussed above..

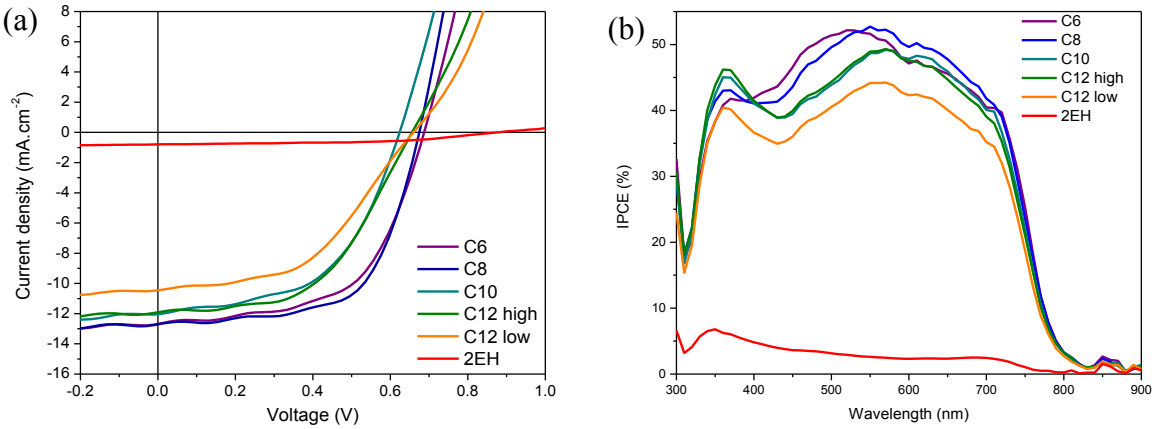

Figure 6. (a) Average J-V curves of BHJ solar cells fabricated from P[T3(R)-iI] derivatives, and (b) characteristic incident photon-to-current efficiency (IPCE) spectra.

Table 4. OPV performance of P[T3(R)-iI] derivatives with $PC_{71}BM$ in devices spun-cast from oDCB.

Polymer: $PC_{71}BM$	Solubility (mg/mL)	Integrated J_{sc} (mA cm^{-2})	J_{sc} (mA cm^{-2})	V_{oc} (V)	FF (%)	PCE (%)	Thickness (nm)
C6	2	11.2	12.3 ± 0.4	0.69 ± 0.01	58 ± 1	5.1 ± 0.1	94 ± 5
C8	10	11.3	12.7 ± 0.3	0.70 ± 0.02	57 ± 5	5.2 ± 0.4	105 ± 6
C10	12	10.6	11.6 ± 0.4	0.63 ± 0.01	54 ± 1	4.1 ± 0.1	113 ± 12
C12 65k	12	10.6	11.3 ± 0.4	0.66 ± 0.00	52 ± 1	4.0 ± 0.1	113 ± 5
C12 41k	21	9.8	11.0 ± 0.4	0.69 ± 0.01	51 ± 1	4.0 ± 0.1	120 ± 2
2EH	27	0.7	0.8 ± 0.1	0.88 ± 0.01	58 ± 3	0.3 ± 0.0	99 ± 12

Statistical data for each polymer performance in OPV was obtained from 12 cells over two separate devices.

As shown in the device current density as a function of voltage curves (Figure 6a) and solubility (Figure S9), and incident photon-to-current efficiency (IPCE) (Figure 6b), the most drastic change is obtained when the polymer backbone includes an all-branched side-chains, leading to an increased open-circuit voltage (V_{oc}), but an order of magnitude lower J_{sc}. Overall, OPV devices based on polymer donors with a P[T3-iI] backbone are relatively insensitive to the linear alkyl side-chain length, and power conversion efficiencies around 5% can be achieved in blends with $PC_{71}BM$ without the use of processing additives. This simple, single solvent processing system also has the added benefit to potentially increase reproducibility of the blend morphology, and resulting device performance, especially between different researchers and laboratories. Work by Duan *et al.* further highlights the interplay between polymer backbone and chain-substitution on device characteristics.[20] In their study based on based on polymers containing benzodithiophene and 5,6-difluorobenzo[2,1,3]thiadiazole, the OPV device performance remains around 4% independent of the alkyl chain length. However, when benzo[2,1,3]thiadiazole is used, polymer substitution with shorter C6 alkyl side chains yields devices with 6% PCE compared to 2% when C10 chains are used.

The change in V_{oc} is related to the higher ionization potential of P[T3(2EH)-iI] compared to the *n*-alkyl derivatives.[42] A first hypothesis for the low J_{sc} could be the low hole mobility measured in OFET devices; however low molecular weight P[T3(C12)-iI] has a hole mobility of the same order of magnitude, but one order of magnitude higher J_{sc}. In order to understand the origin of the low J_{sc} in P[T3(2EH)-iI] devices, the phase separation was imaged via atomic force microscopy as described below.

Phase Separation in BHJ Active Layer. Atomic force microscopy (AFM) is used to gather topological information about the surface of the active layer, with resolutions on the order of tens of nanometers.[66] Therefore, it is important to note that the information discussed based on AFM results may not translate to the bulk morphology of the active layer. Furthermore, although AFM does not directly provide information on the chemical composition at the surface, correlation of TEM and AFM data gathered on isoindigo-based systems,[29] and on donor-acceptor conjugated polymers in general,[21, 36, 67] tends to show (i) polymer-rich fibrillary structures in the active layer or (ii) encapsulation of fullerene-rich domains in a polymer-rich matrix, depending on film composition, material properties and processing conditions. In this study, AFM was employed to image the surface of the active layer and determine the active layer nanoscale topology in polymer:$PC_{71}BM$ thin films (Figure 7). It is expected that varying side-chains will influence polymer solubility in the casting solvent, as well as with fullerene derivatives, and thus influence phase separation. In particular, all films based on polymers with linear side-chains on the terthiophene unit exhibit feature sizes on the order of tens of nm in width, which allows for excitons generated in the polymer domain to diffuse to the fullerene interface and generate short-circuit currents above 11 mA cm^{-2}. In these films, the root-mean-square (rms) roughness is between 2.8 nm and 6.4 nm with little correlation between polymer structure and roughness. Furthermore, there

appears to be little correlation in these systems between polymer solubility and feature sizes as measured by AFM (resolution of tens of nanometers) in contrast to what was previously reported based on TEM results (resolution on the order of nanometers)[37]

However, in the case of P[T3(2EH)-iI] large domains protruding from the surface are formed, leading to a rms roughness of 7.0 nm. Based on previous studies, it is possible that the 2EH AFM image shows islands of $PC_{71}BM$ that are encapsulated by a polymer layer,[31] as was observed with other highly soluble polymers.[21, 29] Mechanistically, it is hypothesized that when π-interactions between polymer chains are possible, fibrillar networks can be formed and limit the growth of $PC_{71}BM$ aggregates.[67] In the case of twisted polymer backbones like P[T3(2EH)-iI], these interchain polymer interactions are limited, possibly leading to liquid-liquid demixing or liquid:solid demixing via fullerene aggregation into large domains prior to any polymer fibril formation,[33] yielding large phase separated domains in the active layer and low J_{sc} in OPV devices.

Interestingly, the phase separation between the polymer and fullerene dominates photocurrent generation over hole mobility in the polymer domains as measured in FET devices. This is observed by comparing the two molecular weight fractions of P[T3(C12)-iI], where high carrier mobilities are not a necessary condition to high OPV device performance, but rather need to be above a certain threshold to achieve high photocurrents, as demonstrated by P[T3(C12)-iI] with a molecular weight of 41 kDa.

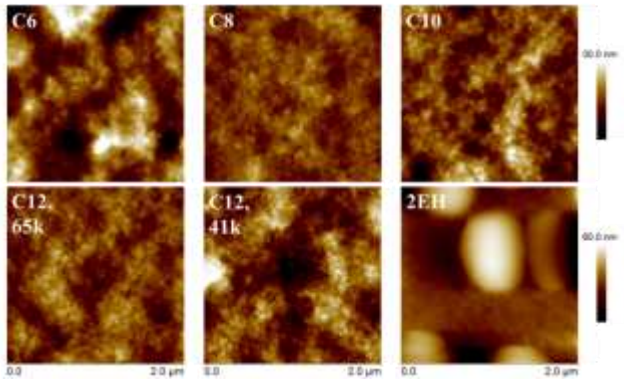

Figure 7. AFM height images of blends of $PC_{71}BM$ blends with P[T3(R)-iI] spun cast from oDCB. R= *n*-hexyl (C6), *n*-octyl (C8), *n*-decyl (C10), *n*-dodecyl (C12, 65k), *n*-dodecyl (C12, 41k), and 2-ethylhexyl (2EH). All images have a 30 nm height scale, except 2EH with 60 nm height scale.

At the nanometer scale, GIWAXS studies on the polymer:fullerene thin films deposited on PEDOT:PSS show similar packing regardless of the P[T3-iI] derivative used (Figure S10). The $PC_{71}BM$ scattering ring can be seen at q values around 1.3-1.4 $Å^{-1}$, in addition to the (h00) peaks from polymer crystallites. A higher order (200) peak can be seen in all GIWAXS images, except in 2EH:$PC_{71}BM$ blends, which is similar to what was observed in Figure 3 for as-cast pure polymer thin films. Overall, scattering from polymer:$PC_{71}BM$ blends is similar to what is observed in as-cast polymer films, although the $PC_{71}BM$ scattering ring obscures the scattering peaks with q values above 1.2 $Å^{-1}$. The chain-to-chain (lamellar) distances within polymer crystallites in blends with $PC_{71}BM$ is comparable to the lamellar distances in the pure polymer films, showing little disruption of the crystalline regions of the polymer domains by $PC_{71}BM$ (Table S3). Quantitatively, the coherence length of the (100) peak along the q_z axis ($L_{c,d}$) is only slightly increased upon addition of $PC_{71}BM$. As such, the differences observed between films based on isoindigo polymers with linear or branched alkyl chains and their subsequent OPV device characteristics are predominantly influenced by the phase separation as observed on the

micrometer scale via AFM (Figure 7). However, the difference in morphology and OPV device parameters within the family of isoindigo polymers with linear side-chains are not only impacted by variations in phase separation, but also by changes in molecular intermixing[68, 69] and crystallinity.[70]

CONCLUSIONS

In this article, we have demonstrated that polymer solubility can be tuned by extending linear alkyl chains, by introducing branching points on the side chain or by varying molecular weight in order to influence polymer packing in thin films. In P[T3(R)-iI] derivatives, GIWAXS shows that linear side-chains on the terthiophene unit promote aggregation as the thin film dries, leading to edge-on orientation of the polymer backbones relative to the substrate and higher order diffraction peaks from the lamellae compared to 2-ethylhexyl side-chains. However, 2D-WAXS also indicates that higher order diffraction peaks for polymers with linear alkyl chains are not necessarily observed in the as-processed polymers, and an increase in ordering is only observed in fibers of P[T3(C6)-iI] after annealing at 200 °C. In contrast to linear chains, branched 2-ethylhexyl chains disrupt π-interactions leading to increased solubility in oDCB and limited ordering at the molecular scale as evidenced by the lack of a low energy shoulder in the solid-state UV-vis absorption spectrum. In OFET devices, changes in polymer morphology are correlated to charge carrier mobility, with some *n*-alkyl derivatives of high molecular weight leading to hole mobilities around 0.02 $cm^2 V^{-1} s^{-1}$ due to increased coherence lengths within the crystallites. Polymers substituted with *n*-octyl chains exhibit a different behavior than other *n*-alkyl-substituted polymers; however the available experimental data does not allow for a conclusion as to why this difference in OFET characteristics arose. In OPV devices the amount of aliphatic chains influences the amount of absorbed light, with derivatives containing longer alkyl chains requiring thicker films (thinner films tend to have

increased fill factors). Short-circuit currents are also slightly affected by changes in the *n*-alkyl side-chain but not as drastically as could have been expected based on the increase in non-conductive volume in the thin films with increased side-chain length. Interestingly, 2-ethylhexyl derivatives show low short-circuit currents but an increased open-circuit voltage. The low J_{sc} can be rationalized by the large domains in phase separation with $PC_{71}BM$, likely due to limited π-interactions, which hinder fibril formation, and to the high solubility of P[T3(2EH)-iI] in oDCB, leaving film morphology to be dominated by the growth of $PC_{71}BM$ aggregates. In contrast, all *n*-alkyl substituted P[T3(R)-iI] showed fibrillar morphology, with feature sizes on the order of tens of nanometers. Overall, P[T3(C8)-iI] has high solubility in oDCB at room temperature and leads to efficiencies around 5% in OPV devices without the use of any processing additives, demonstrating a balance between polymer processability and device performance, which is of increased importance as BHJ transition from spin-coated films to slot-die coated layers.[71] As discussed in the introduction, the propensity for polymer ordering between P[T3-iI] with branched chains and linear chains is comparable to observations made for PBTz4T and PNTz4T systems.[30] Considering differences in polymer structure in terms of backbone symmetry or side-chain steric hindrance, polymer ordering dictates the outcome of polymer crystallization relative to fullerene aggregation and the resulting phase separation in the active layer of OPV devices.

ASSOCIATED CONTENT

Supporting Information. Experimental details, synthetic procedures, polymer characterization (solubility in oDCB, thermal analysis, square-wave voltammograms, GIWAXS and 2D-WAXS

results), OFET and OPV device fabrication and characterization, and gel permeation chromatograms are supplied as Supporting Information.

AUTHOR INFORMATION

Corresponding Author

* Email: reynolds@chemistry.gatech.edu

Present Addresses

†Dow Electronic Materials, Marlborough, Massachusetts 01752, United States.

§ Intel, Hillsboro, Oregon 97124, United States.

‡ Heriot-Watt University, Edinburgh, EH14 4AS, United Kingdom.

Author Contributions

The manuscript was written through contributions of all authors. All authors have given approval to the final version of the manuscript.

Funding Sources

JRR acknowledges funding of this work from the Office of Naval Research (N00014-14-1-0173).

Notes

The authors declare no competing financial interest.

ACKNOWLEDGMENT

JRR acknowledges funding of this work from the Office of Naval Research (N00014-14-1-0173). CG acknowledges the Center for Organic Photonics and Electronics at Georgia Institute of Technology for a fellowship.

REFERENCES

1. Darling, S. B.; You, F. The Case for Organic Photovoltaics. *RSC Adv.* **2013**, *3*, 17633-17648.

2. Grand, C.; Reynolds, J. R. The Interplay between Structure, Processing, and Properties in Organic Photovoltaic Devices: How to Translate Recent Laboratory-Scale Developments to Modules. *MRS Commun.* **2015**, *5*, 155-167.

3. Facchetti, A. π-Conjugated Polymers for Organic Electronics and Photovoltaic Cell Applications. *Chem. Mater.* **2010**, *23*, 733-758.

4. Mei, J.; Diao, Y.; Appleton, A. L.; Fang, L.; Bao, Z. Integrated Materials Design of Organic Semiconductors for Field-Effect Transistors. *J. Am. Chem. Soc.* **2013**, *135*, 6724-6746.

5. Henson, Z. B.; Müllen, K.; Bazan, G. C. Design Strategies for Organic Semiconductors Beyond the Molecular Formula. *Nature Chem.* **2012**, *4*, 699-704.

6. Beaujuge, P. M.; Fréchet, J. M. J. Molecular Design and Ordering Effects in π-Functional Materials for Transistor and Solar Cell Applications. *J. Am. Chem. Soc.* **2011**, *133*, 20009-20029.

7. Mei, J.; Bao, Z. Side Chain Engineering in Solution-Processible Conjugated Polymers for Organic Solar Cells and Field-Effect Transistors. *Chem. Mater.* **2014**, *26*, 604-615.

8. Son, H. J.; Lu, L.; Chen, W.; Xu, T.; Zheng, T.; Carsten, B.; Strzalka, J.; Darling, S. B.; Chen, L. X.; Yu, L. Synthesis and Photovoltaic Effect in Dithieno[2,3-d:2′,3′-d′]Benzo[1,2-b:4,5-b′]dithiophene-Based Conjugated Polymers. *Adv. Mater.* **2013**, *25*, 838-843.

9. Liu, C.; Yi, C.; Wang, K.; Yang, Y.; Bhatta, R. S.; Tsige, M.; Xiao, S.; Gong, X. Single-Junction Polymer Solar Cells with Over 10% Efficiency by a Novel Two-Dimensional Donor–Acceptor Conjugated Copolymer. *ACS Appl. Mater. Interfaces* **2015**, *7*, 4928-4935.

10. Yiu, A. T.; Beaujuge, P. M.; Lee, O. P.; Woo, C. H.; Toney, M. F.; Frechet, J. M. Side-Chain Tunability of Furan-Containing Low-Band-Gap Polymers Provides Control of Structural Order in Efficient Solar Cells. *J. Am. Chem. Soc.* **2012**, *134*, 2180-2185.

11. Meager, I.; Ashraf, R. S.; Mollinger, S.; Schroeder, B. C.; Bronstein, H.; Beatrup, D.; Vezie, M. S.; Kirchartz, T.; Salleo, A.; Nelson, J.; McCulloch, I. Photocurrent Enhancement from Diketopyrrolopyrrole Polymer Solar Cells Through Alkyl-Chain Branching Point Manipulation. *J. Am. Chem. Soc.* **2013**, *135*, 11537-11540.

12. Beaujuge, P. M.; Amb, C. M.; Reynolds, J. R. Spectral Engineering in π-Conjugated Polymers with Intramolecular Donor−Acceptor Interactions. *Acc. Chem. Res.* **2010**, *43*, 1396-1407.

13. Vandewal, K.; Ma, Z.; Bergqvist, J.; Tang, Z.; Wang, E.; Henriksson, P.; Tvingstedt, K.; Andersson, M. R.; Zhang, F.; Inganäs, O. Quantification of Quantum Efficiency and Energy Losses in Low Bandgap Polymer:Fullerene Solar Cells with High Open-Circuit Voltage. *Adv. Funct. Mater.* **2012**, *22*, 3480-3490.

14. Graham, K. R.; Cabanetos, C.; Jahnke, J. P.; Idso, M. N.; El Labban, A.; Ngongang Ndjawa, G. O.; Heumueller, T.; Vandewal, K.; Salleo, A.; Chmelka, B. F.; Amassian, A.; Beaujuge, P. M.; McGehee, M. D. Importance of the Donor:Fullerene Intermolecular Arrangement for High-Efficiency Organic Photovoltaics. *J. Am. Chem. Soc.* **2014**, *136*, 9608-9618.

15. Kim, H.; Lee, B. H.; Lee, K. C.; Kim, G.; Yu, J. Y.; Kim, N.; Lee, S. H.; Lee, K. Role of the Side Chain in the Phase Segregation of Polymer:Fullerene Bulk Heterojunction Composites. *Adv. Energy Mater.* **2013**, *3*, 1575-1580.

16. Kim, G.; Song, S.; Lee, J.; Kim, T.; Lee, T. H.; Walker, B.; Kim, J. Y.; Yang, C. Control of Charge Dynamics via Use of Nonionic Phosphonate Chains and Their Effectiveness for Inverted Structure Solar Cells. *Adv. Energy Mater.* **2015**, *5*, 1500844.

17. Treat, N. D.; Chabinyc, M. L. Phase Separation in Bulk Heterojunctions of Semiconducting Polymers and Fullerenes for Photovoltaics. *Annu. Rev. Phys. Chem.* **2014**, *65*, 59-81.

18. Brabec, C. J.; Heeney, M.; McCulloch, I.; Nelson, J. Influence of Blend Microstructure on Bulk Heterojunction Organic Photovoltaic Performance. *Chem. Soc. Rev.* **2011**, *40*, 1185-1199.

19. Brabec, C. J.; Gowrisanker, S.; Halls, J. J. M.; Laird, D.; Jia, S.; Williams, S. P. Polymer–Fullerene Bulk-Heterojunction Solar Cells. *Adv. Mater.* **2010**, *22*, 3839-3856.

20. Duan, C.; Willems, R. E. M.; van Franeker, J. J.; Bruijnaers, B. J.; Wienk, M. M.; Janssen, R. A. J. Effect of Side Chain Length on the Charge Transport, Morphology, and Photovoltaic Performance of Conjugated Polymers in Bulk Heterojunction Solar Cells. *J. Mater. Chem. A* **2016**, *4*, 1855-1866.

21. Amb, C. M.; Chen, S.; Graham, K. R.; Subbiah, J.; Small, C. E.; So, F.; Reynolds, J. R. Dithienogermole As a Fused Electron Donor in Bulk Heterojunction Solar Cells. *J. Am. Chem. Soc.* **2011**, *133*, 10062-10065.

22. Zhang, Y.; Zou, J.; Yip, H.-L.; Sun, Y.; Davies, J. A.; Chen, K.-S.; Acton, O.; Jen, A. K. Y. Conjugated Polymers Based on C, Si and N-Bridged Dithiophene and Thienopyrroledione Units: Synthesis, Field-Effect Transistors and Bulk Heterojunction Polymer Solar Cells. *J. Mater. Chem.* **2011**, *21*, 3895-3902.

23. Wienk, M. M.; Kroon, J. M.; Verhees, W. J. H.; Knol, J.; Hummelen, J. C.; van Hal, P. A.; Janssen, R. A. J. Efficient Methano[70]fullerene/MDMO-PPV Bulk Heterojunction Photovoltaic Cells. *Angew. Chem., Int. Ed.* **2003**, *42*, 3371-3375.

24. Ye, L.; Zhang, S.; Ma, W.; Fan, B.; Guo, X.; Huang, Y.; Ade, H.; Hou, J. From Binary to Ternary Solvent: Morphology Fine-tuning of D/A Blends in PDPP3T-based Polymer Solar Cells. *Adv. Mater.* **2012**, *24*, 6335-6341.

25. Wang, E.; Ma, Z.; Zhang, Z.; Vandewal, K.; Henriksson, P.; Inganas, O.; Zhang, F.; Andersson, M. R. An Easily Accessible Isoindigo-Based Polymer for High-Performance Polymer Solar Cells. *J. Am. Chem. Soc.* **2011**, *133*, 14244-14247.

26. Guo, X.; Zhou, N.; Lou, S. J.; Hennek, J. W.; Ponce Ortiz, R.; Butler, M. R.; Boudreault, P.-L. T.; Strzalka, J.; Morin, P.-O.; Leclerc, M.; López Navarrete, J. T.; Ratner, M. A.; Chen, L. X.; Chang, R. P. H.; Facchetti, A.; Marks, T. J. Bithiopheneimide–Dithienosilole/Dithienogermole Copolymers for Efficient Solar Cells: Information from Structure–Property–Device Performance Correlations and Comparison to Thieno[3,4-c]pyrrole-4,6-dione Analogues. *J. Am. Chem. Soc.* **2012**, *134*, 18427-18439.

27. Deng, Y.; Liu, J.; Wang, J.; Liu, L.; Li, W.; Tian, H.; Zhang, X.; Xie, Z.; Geng, Y.; Wang, F. Dithienocarbazole and Isoindigo Based Amorphous Low Bandgap Conjugated Polymers for Efficient Polymer Solar Cells. *Adv. Mater.* **2014**, *26*, 471-476.

28. Guo, X.; Zhang, M.; Tan, J.; Zhang, S.; Huo, L.; Hu, W.; Li, Y.; Hou, J. Influence of D/A Ratio on Photovoltaic Performance of a Highly Efficient Polymer Solar Cell System. *Adv. Mater.* **2012**, *24*, 6536-6541.

29. Stalder, R.; Grand, C.; Subbiah, J.; So, F.; Reynolds, J. R. An Isoindigo and Dithieno[3,2-b:2',3'-d]silole Copolymer for Polymer Solar Cells. *Polym. Chem.* **2012**, *3*, 89-92.

30. Osaka, I.; Shimawaki, M.; Mori, H.; Doi, I.; Miyazaki, E.; Koganezawa, T.; Takimiya, K. Synthesis, Characterization, and Transistor and Solar Cell Applications of a

Naphthobisthiadiazole-Based Semiconducting Polymer. *J. Am. Chem. Soc.* **2012**, *134*, 3498-3507.

31. Kouijzer, S.; Michels, J. J.; van den Berg, M.; Gevaerts, V. S.; Turbiez, M.; Wienk, M. M.; Janssen, R. A. J. Predicting Morphologies of Solution Processed Polymer:Fullerene Blends. *J. Am. Chem. Soc.* **2013**, *135*, 12057-12067.

32. Pearson, A. J.; Wang, T.; Dunbar, A. D. F.; Yi, H.; Watters, D. C.; Coles, D. M.; Staniec, P. A.; Iraqi, A.; Jones, R. A. L.; Lidzey, D. G. Morphology Development in Amorphous Polymer:Fullerene Photovoltaic Blend Films During Solution Casting. *Adv. Funct. Mater.* **2014**, *24*, 659-667.

33. van Franeker, J. J.; Turbiez, M.; Li, W.; Wienk, M. M.; Janssen, R. A. J. A Real-Time Study of the Benefits of Co-Solvents in Polymer Solar Cell Processing. *Nature Commun.* **2015**, *6*, 6229.

34. Shin, N.; Richter, L. J.; Herzing, A. A.; Kline, R. J.; DeLongchamp, D. M. Effect of Processing Additives on the Solidification of Blade-Coated Polymer/Fullerene Blend Films via In-Situ Structure Measurements. *Adv. Energy Mater.* **2013**, *3*, 938-948.

35. Richter, L. J.; DeLongchamp, D. M.; Bokel, F. A.; Engmann, S.; Chou, K. W.; Amassian, A.; Schaible, E.; Hexemer, A. In Situ Morphology Studies of the Mechanism for Solution Additive Effects on the Formation of Bulk Heterojunction Films. *Adv. Energy Mater.* **2015**, *5*, 1400975.

36. Li, W.; Hendriks, K. H.; Furlan, A.; Roelofs, W. S. C.; Meskers, S. C. J.; Wienk, M. M.; Janssen, R. A. J. Effect of the Fibrillar Microstructure on the Efficiency of High Molecular Weight Diketopyrrolopyrrole-Based Polymer Solar Cells. *Adv. Mater.* **2014**, *26*, 1565-1570.

37. Li, W.; Hendriks, K. H.; Furlan, A.; Roelofs, W. S. C.; Wienk, M. M.; Janssen, R. A. J. Universal Correlation between Fibril Width and Quantum Efficiency in Diketopyrrolopyrrole-Based Polymer Solar Cells. *J. Am. Chem. Soc.* **2013**, *135*, 18942-18948.

38. Liang, Y.; Yu, L. A New Class of Semiconducting Polymers for Bulk Heterojunction Solar Cells with Exceptionally High Performance. *Acc. Chem. Res.* **2010**, *43*, 1227-1236.

39. Ma, Z.; Sun, W.; Himmelberger, S.; Vandewal, K.; Tang, Z.; Bergqvist, J.; Salleo, A.; Andreasen, J. W.; Inganas, O.; Andersson, M. R.; Muller, C.; Zhang, F.; Wang, E. Structure-Property Relationships of Oligothiophene-Isoindigo Polymers for Efficient Bulk-Heterojunction Solar Cells. *Energy Environ. Sci.* **2014**, *7*, 361-369.

40. Ho, C.-C.; Chen, C.-A.; Chang, C.-Y.; Darling, S. B.; Su, W.-F. Isoindigo-Based Copolymers for Polymer Solar Cells with Efficiency Over 7%. *J. Mater. Chem. A* **2014**, *2*, 8026-8032.

41. Stalder, R.; Puniredd, S. R.; Hansen, M. R.; Koldemir, U.; Grand, C.; Zajaczkowski, W.; Müllen, K.; Pisula, W.; Reynolds, J. R. Ambipolar Charge Transport in Isoindigo-Based Donor–Acceptor Polymers. *Chem. Mater.* **2016**, *28*, 1286-1297.

42. Ko, S.; Hoke, E. T.; Pandey, L.; Hong, S.; Mondal, R.; Risko, C.; Yi, Y.; Noriega, R.; McGehee, M. D.; Brédas, J.-L.; Salleo, A.; Bao, Z. Controlled Conjugated Backbone Twisting for an Increased Open-Circuit Voltage while Having a High Short-Circuit Current in Poly(hexylthiophene) Derivatives. *J. Am. Chem. Soc.* **2012**, *134*, 5222–5232.

43. Cardona, C. M.; Li, W.; Kaifer, A. E.; Stockdale, D.; Bazan, G. C. Electrochemical Considerations for Determining Absolute Frontier Orbital Energy Levels of Conjugated Polymers for Solar Cell Applications. *Adv. Mater.* **2011**, *23*, 2367-2371.

44. Zhang, X.; Richter, L. J.; DeLongchamp, D. M.; Kline, R. J.; Hammond, M. R.; McCulloch, I.; Heeney, M.; Ashraf, R. S.; Smith, J. N.; Anthopoulos, T. D.; Schroeder, B.; Geerts, Y. H.; Fischer, D. A.; Toney, M. F. Molecular Packing of High-Mobility Diketo Pyrrolo-Pyrrole Polymer Semiconductors with Branched Alkyl Side Chains. *J. Am. Chem. Soc.* **2011**, *133*, 15073-15084.

45. Mei, J.; Kim do, H.; Ayzner, A. L.; Toney, M. F.; Bao, Z. Siloxane-Terminated Solubilizing Side Chains: Bringing Conjugated Polymer Backbones Closer and Boosting Hole Mobilities in Thin-Film Transistors. *J. Am. Chem. Soc.* **2011**, *133*, 20130-20133.

46. Rivnay, J.; Steyrleuthner, R.; Jimison, L. H.; Casadei, A.; Chen, Z.; Toney, M. F.; Facchetti, A.; Neher, D.; Salleo, A. Drastic Control of Texture in a High Performance n-Type Polymeric Semiconductor and Implications for Charge Transport. *Macromolecules* **2011**, *44*, 5246-5255.

47. Chen, M. S.; Lee, O. P.; Niskala, J. R.; Yiu, A. T.; Tassone, C. J.; Schmidt, K.; Beaujuge, P. M.; Onishi, S. S.; Toney, M. F.; Zettl, A.; Frechet, J. M. Enhanced Solid-State Order and Field-Effect Hole Mobility Through Control of Nanoscale Polymer Aggregation. *J. Am. Chem. Soc.* **2013**, *135*, 19229-19236.

48. Lu, C.; Chen, H.-C.; Chuang, W.-T.; Hsu, Y.-H.; Chen, W.-C.; Chou, P.-T. Interplay of Molecular Orientation, Film Formation, and Optoelectronic Properties on Isoindigo- and Thienoisoindigo-Based Copolymers for Organic Field Effect Transistor and Organic Photovoltaic Applications. *Chem. Mater.* **2015**, *27*, 6837-6847.

49. Kim, Y.; Long, D. X.; Lee, J.; Kim, G.; Shin, T. J.; Nam, K.-W.; Noh, Y.-Y.; Yang, C. A Balanced Face-On to Edge-On Texture Ratio in Naphthalene Diimide-Based Polymers with Hybrid Siloxane Chains Directs Highly Efficient Electron Transport. *Macromolecules* **2015**, *48*, 5179-5187.

50. Sirringhaus, H. 25th Anniversary Article: Organic Field-Effect Transistors: The Path Beyond Amorphous Silicon. *Adv. Mater.* **2014**, *26*, 1319-1335.

51. Osaka, I.; Takimiya, K. Backbone Orientation in Semiconducting Polymers. *Polymer* **2015**, *59*, A1-A15.

52. Cho, E.; Risko, C.; Kim, D.; Gysel, R.; Cates Miller, N.; Breiby, D. W.; McGehee, M. D.; Toney, M. F.; Kline, R. J.; Bredas, J.-L. Three-Dimensional Packing Structure and Electronic Properties of Biaxially Oriented Poly(2,5-bis(3-alkylthiophene-2-yl)thieno[3,2-b]thiophene) Films. *J. Am. Chem. Soc.* **2012**, *134*, 6177-6190.

53. Rivnay, J.; Toney, M. F.; Zheng, Y.; Kauvar, I. V.; Chen, Z.; Wagner, V.; Facchetti, A.; Salleo, A. Unconventional Face-On Texture and Exceptional In-Plane Order of a High Mobility n-Type Polymer. *Adv. Mater.* **2010**, *22*, 4359-4363.

54. Rivnay, J.; Mannsfeld, S. C. B.; Miller, C. E.; Salleo, A.; Toney, M. F. Quantitative Determination of Organic Semiconductor Microstructure from the Molecular to Device Scale. *Chem. Rev.* **2012**, *112*, 5488-5519.

55. Rogers, J. T.; Schmidt, K.; Toney, M. F.; Kramer, E. J.; Bazan, G. C. Structural Order in Bulk Heterojunction Films Prepared with Solvent Additives. *Adv. Mater.* **2011**, *23*, 2284-2288.

56. Kim, G.; Han, A. R.; Lee, H. R.; Oh, J. H.; Yang, C. Use of Heteroaromatic Spacers in Isoindigo-Benzothiadiazole Polymers for Ambipolar Charge Transport. *Phys. Chem. Chem. Phys.* **2015**, *17*, 26512-26518.

57. Beaujuge, P. M.; Tsao, H. N.; Hansen, M. R.; Amb, C. M.; Risko, C.; Subbiah, J.; Choudhury, K. R.; Mavrinskiy, A.; Pisula, W.; Brédas, J.-L.; So, F.; Müllen, K.; Reynolds, J. R. Synthetic Principles Directing Charge Transport in Low-Band-Gap Dithienosilole–Benzothiadiazole Copolymers. *J. Am. Chem. Soc.* **2012**, *134*, 8944-8957.

58. Noriega, R.; Rivnay, J.; Vandewal, K.; Koch, F. P. V.; Stingelin, N.; Smith, P.; Toney, M. F.; Salleo, A. A General Relationship Between Disorder, Aggregation and Charge Transport in Conjugated Polymers. *Nature Mater.* **2013**, *12*, 1038–1044.

59. Zhang, X.; Bronstein, H.; Kronemeijer, A. J.; Smith, J.; Kim, Y.; Kline, R. J.; Richter, L. J.; Anthopoulos, T. D.; Sirringhaus, H.; Song, K.; Heeney, M.; Zhang, W.; McCulloch, I.; DeLongchamp, D. M. Molecular Origin of High Field-Effect Mobility in an Indacenodithiophene–Benzothiadiazole Copolymer. *Nature Commun.* **2013**, *4*, 2238.

60. Venkateshvaran, D.; Nikolka, M.; Sadhanala, A.; Lemaur, V.; Zelazny, M.; Kepa, M.; Hurhangee, M.; Kronemeijer, A. J.; Pecunia, V.; Nasrallah, I.; Romanov, I.; Broch, K.; McCulloch, I.; Emin, D.; Olivier, Y.; Cornil, J.; Beljonne, D.; Sirringhaus, H. Approaching Disorder-Free Transport in High-Mobility Conjugated Polymers. *Nature* **2014**, *515*, 384-388.

61. Park, W.-T.; Kim, G.; Yang, C.; Liu, C.; Noh, Y.-Y. Effect of Donor Molecular Structure and Gate Dielectric on Charge-Transporting Characteristics for Isoindigo-Based Donor–Acceptor Conjugated Polymers. *Adv. Funct. Mater.* **2016**, *26*, 4695-4703.

62. Baker, J. L.; Jimison, L. H.; Mannsfeld, S.; Volkman, S.; Yin, S.; Subramanian, V.; Salleo, A.; Alivisatos, A. P.; Toney, M. F. Quantification of Thin Film Crystallographic Orientation Using X-ray Diffraction with an Area Detector. *Langmuir* **2010**, *26*, 9146-9151.

63. Grand, C.; Baek, S.; Lai, T.-H.; Deb, N.; Zajaczkowski, W.; Stalder, R.; Müllen, K.; Pisula, W.; Bucknall, D. G.; So, F.; Reynolds, J. R. Structure–Property Relationships Directing Transport and Charge Separation in Isoindigo Polymers. *Macromolecules* **2016**, *49*, 4008-4022.

64. Guerrero, A.; Montcada, N. F.; Ajuria, J.; Etxebarria, I.; Pacios, R.; Garcia-Belmonte, G.; Palomares, E. Charge Carrier Transport and Contact Selectivity Limit the Operation of PTB7-

Based Organic Solar Cells of Varying Active Layer Thickness. *J. Mater. Chem. A* **2013**, *1*, 12345-12354.

65. Small, C. E.; Tsang, S.-W.; Chen, S.; Baek, S.; Amb, C. M.; Subbiah, J.; Reynolds, J. R.; So, F. Loss Mechanisms in Thick-Film Low-Bandgap Polymer Solar Cells. *Adv. Energy Mater.* **2013**, *3*, 909-916.

66. Chen, W.; Nikiforov, M. P.; Darling, S. B. Morphology Characterization in Organic and Hybrid Solar Cells. *Energy Environ. Sci.* **2012**, *5*, 8045-8074.

67. Hoppe, H.; Sariciftci, N. S. Morphology of Polymer/Fullerene Bulk Heterojunction Solar Cells. *J. Mater. Chem.* **2006**, *16*, 45-61.

68. Yau, C. P.; Fei, Z.; Ashraf, R. S.; Shahid, M.; Watkins, S. E.; Pattanasattayavong, P.; Anthopoulos, T. D.; Gregoriou, V. G.; Chochos, C. L.; Heeney, M. Influence of the Electron Deficient Co-Monomer on the Optoelectronic Properties and Photovoltaic Performance of Dithienogermole-based Co-Polymers. *Adv. Funct. Mater.* **2014**, *24*, 678-687.

69. Shao, M.; Keum, J. K.; Kumar, R.; Chen, J.; Browning, J. F.; Das, S.; Chen, W.; Hou, J.; Do, C.; Littrell, K. C.; Rondinone, A.; Geohegan, D. B.; Sumpter, B. G.; Xiao, K. Understanding How Processing Additives Tune the Nanoscale Morphology of High Efficiency Organic Photovoltaic Blends: From Casting Solution to Spun-Cast Thin Film. *Adv. Funct. Mater.* **2014**, *24*, 6647-6657.

70. Sweetnam, S.; Graham, K. R.; Ngongang Ndjawa, G. O.; Heumüller, T.; Bartelt, J. A.; Burke, T. M.; Li, W.; You, W.; Amassian, A.; McGehee, M. D. Characterization of the Polymer Energy Landscape in Polymer:Fullerene Bulk Heterojunctions with Pure and Mixed Phases. *J. Am. Chem. Soc.* **2014**, *136*, 14078-14088.

71. Ro, H. W.; Downing, J. M.; Engmann, S.; Herzing, A. A.; DeLongchamp, D. M.; Richter, L. J.; Mukherjee, S.; Ade, H.; Abdelsamie, M.; Jagadamma, L. K.; Amassian, A.; Liu, Y. H.; Yan, H. Morphology Changes Upon Scaling a High-Efficiency, Solution-Processed Solar Cell. *Energy Environ. Sci.* **2016**, *9*, 2835-2846.

72. Peet, J.; Kim, J. Y.; Coates, N. E.; Ma, W. L.; Moses, D.; Heeger, A. J.; Bazan, G. C. Efficiency Enhancement in Low-Bandgap Polymer Solar Cells by Processing with Alkane Dithiols. *Nature Mater.* **2007**, *6*, 497-500.

73. Park, S. H.; Roy, A.; Beaupre, S.; Cho, S.; Coates, N.; Moon, J. S.; Moses, D.; Leclerc, M.; Lee, K.; Heeger, A. J. Bulk Heterojunction Solar Cells with Internal Quantum Efficiency Approaching 100%. *Nature Photon.* **2009**, *3*, 297-302.

74. Wan, M.; Zhu, H.; Deng, H.; Jin, L.; Guo, J.; Huang, Y. Low Band-Gap Modulation of Isoindigo-Based Copolymers Toward High Open-Circuit Voltage of Polymer Solar Cells. *J. Polym. Sci., Part A: Polym. Chem.* **2013**, *51*, 3477-3485.

For Table of Contents use only: